Bioorganic Chemistry 112 (2021) 104912

Contents lists available at ScienceDirect

Bioorganic Chemistry

journal homepage: www.elsevier.com/locate/bioorg

Identification of novel anti-inflammatory Nur77 modulators by virtual screening

Xiaoyu Ding [b,d,1], Zijie Zhao [b,c,d,1], Yue Wu [b,d,1], Hao Zhang [b], Kaixian Chen [b,c,d], Cheng Luo [a,b,d,*], Xiaomin Luo [b,d,*], Heng Xu [a,b,*]

[a] School of Pharmaceutical Science and Technology, Hangzhou Institute for Advanced Study, University of Chinese Academy of Sciences, Hangzhou 310000, China
[b] Drug Discovery and Design Center, State Key Laboratory of Drug Research, Shanghai Institute of Materia Medica, Chinese Academy of Sciences, 555 Zuchongzhi Road, Shanghai 201203, China
[c] Shanghai Institute for Advanced Immunochemical Studies, and School of Life Science and Technology, ShanghaiTech University, Shanghai 200031, China
[d] University of Chinese Academy of Sciences, 19 Yuquan Road, Beijing 100049, China

ARTICLE INFO

Keywords:
Nur77
Binding site evaluation
Virtual Screening
Inflammation

ABSTRACT

Orphan nuclear receptor Nur77 is a unique member of the NR4A nuclear receptor subfamily, which is critical for cellular processes especially the inflammatory responses. Many efforts have been made to discover novel scaffold small molecules targeting Nur77. Herein, we evaluated the previously reported binding sites in crystal structures of Nur77 with small molecules, and then discovered compound **13** as a hit of Nur77 via virtual screening targeting the best-scored binding site. Based on the results of fluorescence titration assay, structure–activity relationship (SAR) analysis was summarized for compound **13** and its analogs. Among these analogs, compound **13e** displayed the most potent binding affinity (0.54 ± 0.02 μM). The binding mode of compound **13e** was predicted via molecule docking. Moreover, **13e** exhibited significant anti-inflammation activity in TNF-α induced HepG2 cell model. Taken together, these results provided a new insight into the understanding the functions of specific binding sites on Nur77 for small molecular compounds, and the development of new scaffold Nur77 modulators.

1. Introduction

Orphan nuclear receptor Nur77 (also known as NR4A1/TR3/NGFIB) is a unique member of the NR4A nuclear receptor subfamily and a key regulator of various signaling transduction pathways. Mediating a broad spectrum of physiological functions including cell proliferation, differentiation, apoptosis, and autophagy, Nur77 is implicated in multiple diseases such as cancer, metabolic diseases, and inflammatory diseases. Both *in vitro* and *in vivo* evidence show that Nur77 is involved in the immune response to protein inflammatory stimuli, such as tumor necrosis factor-α (TNF-α), Toll-like receptor ligands, and oxidized lipids [1]. Moreover, studies have suggested the potential of Nur77 to alleviate various inflammatory diseases [2,3]. In conclusion, Nur77 is an attractive and promising drug target for inflammatory disease therapies.

In terms of protein structure, Nur77 consists of an *N*-terminal domain, a DNA binding domain, and a ligand-binding domain, which is the typical structure of a nuclear receptor. Nur77 was first identified as an orphan receptor, the endogenous ligand of which has not yet been found. However, an increasing number of small molecules targeting Nur77 have been reported to regulate the biological functions of Nurr77. To date, several categories of Nur77 modulators have been discovered [2,4], such as Cytosporone B (Csn-B) and its analogs [5-8], Methylene-substituted diindolylmethanes (C-DIMs)[9-17], Celastrol and its analogs [18,19], and *n*-Butylidenephthalide (BP) and its derivative [20-23]. Given their limited structural diversity and optimization prospects, it is therefore of high interest to discover Nur77 modulators with novel scaffolds. Notably, the majority of Nur77 modulators were investigated for the treatment of cancer, while less explored for their anti-inflammatory efficacy. Thus, it is important to discover Nur77 targeting compounds that are beneficial to the clinical treatment of inflammation related disease.

As a common approach to discover molecule modulators with novel scaffolds, virtual screening was used to screen out novel hit compounds of Nur77. For instance, small molecule ligand ethyl 2-[2,3,4-trimethoxy-

* Corresponding authors at: School of Pharmaceutical Science and Technology, Hangzhou Institute for Advanced Study, University of Chinese Academy of Sciences, Hangzhou 310000, China.
E-mail addresses: cluo@simm.ac.cn (C. Luo), xmluo@simm.ac.cn (X. Luo), idaheng@simm.ac.cn (H. Xu).
[1] These authors contributed equally to this work.

https://doi.org/10.1016/j.bioorg.2021.104912
Received 10 December 2020; Received in revised form 19 March 2021; Accepted 7 April 2021
Available online 20 April 2021
0045-2068/© 2021 Elsevier Inc. All rights reserved.

6-(1-octanoyl)phenyl]acetate (TMPA) was discovered via virtual screening technology [24]. Another NR4A1 antagonist 2-imino-6-methoxy-2H-chromene-3-carbothioamide (IMCA) was identified via structure-guided virtual screening based on the crystal structure of Nur77-TMPA complex and was demonstrated as an anticancer drug candidate for thyroid carcinoma chemotherapy [25]. Since several small molecule binding sites have been revealed in previously reported crystal structures of Nur77, we have assessed these binding sites via the SiteMap (version 3.4) module from the Schrödinger software. Then site-specific virtual screening was carried out based on the best scored small molecule binding site.

In this work, a promising hit compound **13** was discovered via virtual screening. Similarity-based searching was then performed for the optimization of this hit compound, as well as to study the structure–activity relationship (SAR) of these new scaffold Nur77 modulators, among which compound **13e** was evaluated for its anti-inflammatory effects. These results indicated that compound **13e** with a K_d value of 0.54 ± 0.02 μM might serve as a starting point for further optimization.

2. Methods

2.1. Small molecule binding sites evaluation

2.1.1. Protein preparation

The crystal structures of Nur77 were retrieved from the Protein Data Bank (PDB id: 3V3Q [24], 4KZI [26], 4RZG [27], 4WHG [28], 6KZ5 [29]). The protein structures were prepared in the Protein Preparation Wizard Workflow of the Schrödinger software package (Schrödinger LLC, New York, NY, 2010). All crystal water and glycerol molecules were deleted from the complex structures, and hydrogens were added. Each complex was then minimized with the OPLS_2005 force field and a maximum RMSD of 0.30 Å to restrain steric clashes. Subsequently, a three-dimensional receptor grid was generated using the Receptor Grid Generation module from the Maestro software (Maestro, version 9.1; Schrödinger LLC, New York, NY, 2010) on the size and centroid of the respective ligands. The values were assigned to default for the other parameters.

2.1.2. Binding sites evaluation by SiteMap

We employed the SiteMap module of Maestro (version 3.4, Schrödinger LLC, New York, NY, 2010) to evaluate the binding site regions. 6 Å regions around the respective small molecule of each Nur77 crystal structure was selected as default. The number of site points was set to 15 as default. More restrictive hydrophobicity was defined as default, and the fine grid mode was used. Other parameters were set as default.

2.2. Structure-based virtual screening

2.2.1. Ligand preparation

In total, about 1,400,000 compounds from the ChemDiv database (https://www.chemdiv.com) were used. Compounds containing pan-assay interference structure (PAINS) or violating "Lipinski's Rule of Five" were removed from the compound library. Then LigPrep (version 2.4, Schrödinger, LLC, New York, NY, 2010) was used to generate stereoisomers and tautomer, and the stereoisomers were generated at most 32 per ligand. The protonation states of ligands at pH 7.0 ± 2.0 were generated with Epik [30]. Then generated structures were used for subsequent docking procedures.

2.2.2. Glide docking procedure

The prepared receptor and ligand files were imported into the Ligand Docking module using the Glide module of Maestro software (Glide, version 6; Schrödinger LLC, New York, NY, 2010) with the standard precision mode (SP). The top-ranked 1,000 poses were chosen to group into 50 clusters using our in-house script. The similarity between two compounds was calculated using the Tanimoto coefficient of ECFP4 fingerprint. After visual inspection of the binding poses of these compounds, 39 molecules with structural diversity and shape rationality were selected and purchased for further biological assay evaluation.

2.2.3. Similarity-based analog searching

In order to obtain derivatives of hit compounds, the ChemDiv database filtered with PAINS was searched using our in-house script. The similarity between two compounds was calculated using the Tanimoto coefficient of ECFP4 fingerprint. The similarity cutoff was set to 0.4, and 7 analogs in stock were found by the threshold of similarity and purchased for further evaluation.

2.2.4. Commercial compounds

Compounds were purchased from the ChemDiv Company (San Diego, CA, USA). The purities of all compounds are above 95% and compounds were used directly without further purification. All compounds were dissolved in DMSO for all assays.

2.3. Protein expression and purification

The sequence of Nur77-LBD (ligand-binding domain) was inserted into pET-22b expression vector and Nurr1-LBD was inserted into pET-15b expression vector. The proteins were overexpressed in *Escherichia coli* BL21 (DE3) strain. Cells were cultured at 37 ℃ for 5 h and induced with 500 mM isopropyl β-D-1-thiogalactopyranoside (IPTG) at 16 ℃ overnight. The cells were harvested by centrifugation at 4000 rpm for 20 min and lysed by sonification in buffer A (20 mM Tris-HCl pH 8.5, 200 mM NaCl, 0.05% β-ME). After centrifugation, the supernatant was loaded onto Histrap HP columns (GE Healthcare) and the protein was eluted with a gradient of imidazole (0 to 500 mM) in buffer A. The elution fractions were pooled and further purified by gel filtration Superdex 75 increase column (GE Healthcare) in buffer B (20 mM Tris-HCl pH 8.5, 200 mM NaCl). Each fraction was examined by SDS-PAGE. Purified protein was concentrated to the appropriate concentration and stored in buffer B with extra 5% glycerin at −80 ℃ used for subsequent assays.

2.4. Protein thermal shift (PTS) assay

The thermal stability of Nur77 was detected using the QuantStudio™ 6 Flex Real-time PCR system. Compounds (400 μM) were incubated with 20 μM Nur77-LBD and 5 × SYPRO orange (Invitrogen) in assay buffer (20 mM Tris-HCl pH 8.5, 200 mM NaCl). The fluorescence signal was collected from 25 ℃ to 95 ℃ within 25 min. The variation of T_m was calculated by the Protein Thermal Shift™ Software version 1.2 and then processed using the GraphPad Prism 5.0 (GraphPad Software, La Jolla, CA, USA).

2.5. Fluorescence quenching assay

Nur77-LBD or Nurr1-LBD protein (1 μM in Phosphate-Buffered Saline (PBS)) was mixed with different concentrations of compounds (from 0 μM to 45 μM, solved in DMSO and diluted in PBS) in 384 microplates. The difference between each concentration keeps the same value (5 μM). After incubation for 40 min at room temperature, the proteins with DMSO were excited at 280 nm and the fluorescence signal was recorded from 280 nm to 360 nm. According to the fluorescence spectra of Nur77 and Nurr1, the fluorescence peak was located at 330 nm for Nur77 and 334 nm for Nurr1. Thus, the proteins were excited at 280 nm and emission at 330 nm or 334 nM. Data were processed by the GraphPad Prism 5.0 according to the one-site binding model.

2.6. Surface plasmon resonance (SPR) assay

Surface plasmon resonance assay was performed using the Biacore

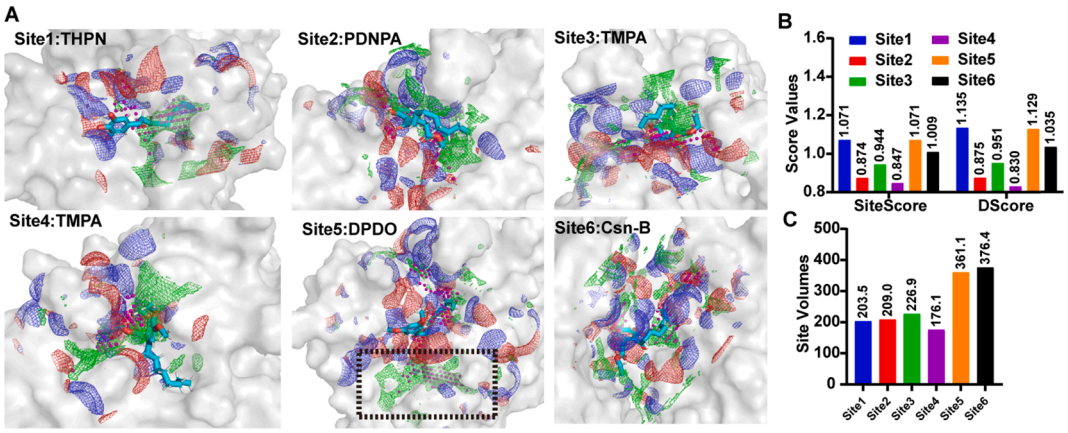

Fig. 1. Evaluation of small molecule binding sites of Nur77. (A) Small molecule binding sites of Nur77. Site1 is the binding site of THPN (PDB id: 4WHG); Site2 is the binding site of PDNPA (PDB id: 4RZG); Site3 and Site4 are the binding sites of TMPA (PDB id: 3V3Q); Site5 is the binding site of DPDO (PDB id: 4KZI); Site6 is the binding site of Csn-B (PDB id:6KZ5). The hydrogen bond acceptor areas are colored in red; the hydrogen bond donor areas are colored in blue; the hydrophobic areas are colored in green; the site points are colored in magenta. (B) The SiteScores and DScores of all six sites. (C) Site volumes of all six sites. (For interpretation of the references to colour in this figure legend, the reader is referred to the web version of this article.)

T200 instrument according to manufacturer's instruction. Recombinant Nur77-LBD protein was coupled to CM5 sensor chip (GE Healthcare). The final immobilization response of Nur77-LBD was 4500 resonance units. The path without protein coupling was used as the reference, to deduct the background signal. Different concentrations of compounds were injected at the flow rate of 20 μL/min to bind with immobilized proteins, and the response units were monitored in real-time. Each cycle consists of association phase (60–180 s) and disassociation phase (after 180 s), which represent the binding between compounds and proteins, and the binding compounds were washed off from the protein surface, respectively. The data was processed using the Biacore T200 Evaluation software Version 1.0.

2.7. Cell culture

Human hepatocellular carcinoma cell lines HepG2 was purchased from the American Type Culture Collection (ATCC) and maintained in Dulbecco's Modified Eagle Medium (Gibco) containing 10% fetal bovine serum (Gibco) and 1% antibiotics (penicillin and streptomycin). All cells were incubated at 37 °C under 5% (v/v) CO_2 atmosphere.

2.8. Cytotoxicity assay

The HepG2 were cultured into a 96-well plate for 24 h and then treated with a gradient concentration of compound for 72 h. Then 20 μL CellTiter-Glo reagent (Promega) was added to each well. After incubation for 20 min, the luminescence was measured by EnVision (Perkin Elmer). Data were processed using the GraphPad Prism 5.0.

2.9. The extraction of nuclear and cytoplasmic

Cells were collected after treated with compound **13e** for 6 h and TNF-α for 20 min. Cells were resuspended with Buffer A (10 mM Hepes pH 7.9, 5 mM $MgCl_2$, 0.25 M Sucrose, 0.1% NP-40 (v/v)) and placed on ice for 20 min. After centrifuging at 9800 × g in 4℃ for 15 min, and the supernatant was collected as cytosolic. Buffer B (25 mM Hepes pH 7.9, 20%, glycerol, 1.5 mM $MgCl_2$, 0.1 mM EDTA, 700 mM NaCl) was added to the pellets. After incubating with Buffer B on ice for 10 min, the homogenates were sonicated on ice until liquidly. The homogenates were centrifuged at 15000 × g in 4℃ for 15 min, and the supernatant was collected as nuclear.

2.10. Western blotting

The HepG2 cells were treated with different concentrations of compounds in DMEM without FBS for 6 h and stimulated by TNF-α for an extra 20 min. Cells were lysed by lysis buffer (100 mM Tris-HCl, pH 6.8, 4% SDS (w/v), 0.2% BPB (w/v), 20% glycerin (v/v), 2% β-ME (w/v)) at 99 ℃ for 15 min. Proteins were separated by SDS-polyacrylamide gel electrophoresis from cell lysate and then the target protein was transferred onto 0.45 mm nitrocellulose membranes. After blocked by 5% non-fat milk (solved in TBST) for 1 h at room temperature, membranes were incubated with corresponding primary antibodies overnight at 4 ℃. Secondary antibodies were subsequently applied for another 1 h at room temperature. After washed by TBST for 3 times, all the protein bands were eventually detected by Amersham Imager 600 (GE Healthcare).

Primary antibodies: anti-IκBα (Cell Signaling Technology, #4814), anti-α-Tubulin (Cell Signaling Technology, #2144).

Secondary antibodies: HRP-conjugated Goat Anti-Mouse IgG (BBI, D110087), HRP-conjugated Goat Anti-Rabbit IgG (BBI, D110058).

2.11. Real-time quantitative PCR

HepG2 cells were treated with different concentrations of compounds for 24 h and TNF-α (20 ng/mL) for 8 h. Total RNA was isolated using FastPure® Cell/Tissue Total RNA Isolation Kit V2 (Vazyme, RC112) and reverse transcribed by HiScript II Q RT SuperMix (Vazyme, R223-01) according to manufacturer's instruction. Real-time quantitative PCR was performed using ChamQ SYBR qPCR Master Mix (Vazyme, Q331-02) in QuantStudio™ 6 Flex Real-Time PCR System (Thermal Fisher) according to the manufacturer's instruction. The profile of thermal cycling consisted of initial denaturation at 95 °C for 30 s, and 40 cycles at 95 °C for 5 s and 60 °C for 30 s. The specificity of primers was examined by melting curve analysis. GAPDH mRNA levels were used as an inner reference for normalization. The primers were as below:

Human TNF-α forward: GTCAACCTCCTCTCTGCCATCAAG
Human TNF-α reverse: CTGAGTCGGTCACCCTTCTCCA
Human GAPDH forward: GAAGGTCGGAGTCAACGGAT
Human GAPDH reverse: CCTGGAAGATGGTGATGGG

3. Results and discussion

3.1. Small molecule binding sites evaluation.

After inspection of all the co-crystal structures of Nur77 with small

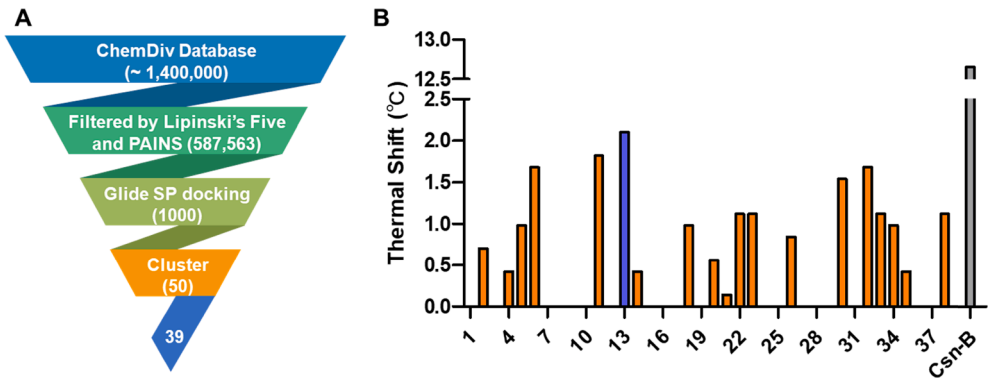

Fig. 2. Discovery of the hit compound **13** of Nur77. (A) The workflow of virtual screening. (B) The protein thermal shift assay results of 39 compounds. Csn-B was used as the positive control. The thermal shift values were referenced to the control group of Nur77 protein incubated with DMSO.

molecules, we found that six distinct small molecule binding sites of Nur77 protein have been reported (Fig. 1**A**). Interestingly, although these compounds shared similarities in chemical structures, they displayed independent biological functions via disrupting interactions of different proteins with Nur77[5,24,27,29,31]. To evaluate and compare different binding sites unbiasedly and quickly, Maestro SiteMap was used for the assessment of SiteScore and DScore for each binding site. The SiteScore was calculated based on several properties, such as the volume of sites, hydrogen bonds, hydrophobicity and et ac.[32-34]. A SiteScore > 0.8 means the site is probably a compound binding site. On account of this, all the six binding sites of Nur77 show good properties in compound binding (Fig. 1**B**). A SiteScore of > 1 suggests a site of particular promise, which means the Site1, Site5 and Site6 show good promisity. DScore is the score of druggability of binding sites [32]. Site1 of Nur77 showed the best DScore among all the six sites. Site5 and Site6 displayed apparently larger volume compared to other sites (Fig. 1**C**). Especially, Site5 contained parts of the Site1 area as shown in black dotted rectangle. Different small molecules could bind to different pockets in large binding areas of Site5 or Site6, which could result in distinct biological activities. Therefore, it might be difficult to summarize structure–activity relationship of Site5 or Site6. Considering the two scores and site volumes, Site1 was chosen as the most promise binding site of all. Accordingly, Site1 was utilized in subsequent structure-based high-throughput virtual screening for the discovery of novel scaffold Nur77 targeting compounds.

3.2. *Binding site evaluation based virtual screening and hit compound identification.*

The overall workflow of virtual screening is shown in Fig. 2**A**. The commercially available ChemDiv database containing about 1,400,000 compounds was used as the ligand library. Filtered by Lipinski's rule of five and PAINS, the remaining 587,563 compounds were prepared and docked into the binding site of the prepared receptor. The top-ranked 1,000 molecules were selected and clustered into 50 groups to eliminate highly similar structures. Accounting for both the structural diversity and shape rationality, 39 molecules were manually selected and purchased for further biological assay evaluation.

Then Protein Thermal Shift assay was used to determine the binding activity of the selected 39 compounds with Nur77 (**Table S1**). The variation of protein T_m values of 39 compounds against Nur77 was depicted in Fig. 2**B**. According to the results, there were 9 compounds showed thermal shift beyond 1 ℃, 4 compounds showed thermal shift beyond 1.5 ℃, and the compound **13** is the only one showed thermal shift beyond 2 ℃ (from 53.17 ℃ to 51.07 ℃). The thermal shift value of positive control (Csn-B) was consistent with the previous study [29]. Therefore, compound **13** was chosen as a hit compound for further optimization.

3.3. *Structure-activity relationship analysis of compound 13 and its derivatives via fluorescence quenching assay*

The binding affinity of compound **13** to Nur77 was further evaluated by fluorescence quenching assay. As previously reported, the fluorescence of Nur77 protein could be quenched measurably if compounds could interact with Nur77 [35,36]. After incubation with Nur77-LBD, the binding affinity of compound **13** was measured. The K_d value was calculated as 4.03 ± 0.85 μM, as shown in Fig. 3.

To explore the structure–activity relationship of this novel scaffold Nur77 targeting compound, derivatives of compound **13** were chosen

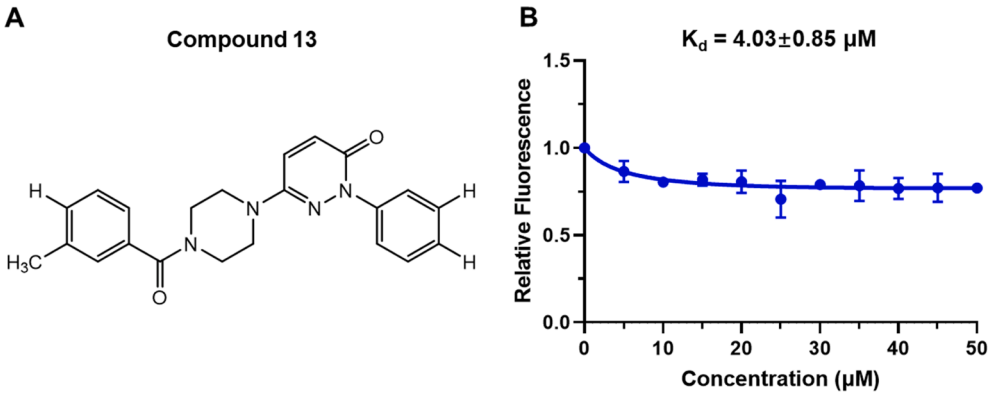

Fig. 3. The *in-vitro* binding affinity of compound **13** to Nur77-LBD. (A) The chemical structure of compound **13**. (B) Nur77-LBD was incubated with different concentrations of **13** in assay buffer for 30 min at room temperature. The fluorescence intensity was measured at the excitation of 280 nm and the emission of 330 nm. Three independent experiments were carried out and the data was processed by the GraphPad Prism 5.0. K_d was shown as mean ± SEM.

Table 1
The binding affinity of compound **13** and its derivatives.

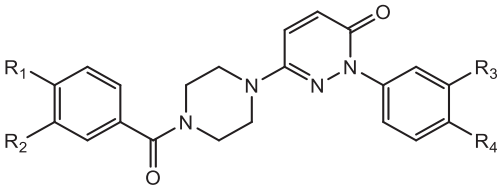

CID	R_1	R_2	R_3	R_4	Binding Affinity (μM)
13	H	CH_3	H	H	4.03 ± 0.85
13a	H	$N(CH_3)_2$	CH_3	CH_3	11.37 ± 1.27
13b	H	Br	CH_3	CH_3	> 50
13c	H	F	CH_3	CH_3	> 50
13d	Cl	H	H	H	> 50
13e	$N(CH_3)_2$	H	H	H	0.54 ± 0.02
13f	Br	H	H	H	> 50
13g	OCH_3	H	H	H	1.99 ± 0.56

via 2D similarity searching. Seven derivatives were measured in fluorescence quenching assay to obtain the binding affinity (**Fig. S1**). The K_d values of 7 derivatives were shown in Table 1. In the comparison of **13e** with **13g** and **13f**, the electron-donating ability of R_1 ($N(CH_3)_2$ > OCH_3 > Br) was consistent with the binding affinity (**13e** > **13g** > **13f**). In the comparison of compound **13a** with **13b**, the electron-donating ability of R_2 ($N(CH_3)_2$ > Br) was consistent with the binding affinity (**13a** > **13b**) as well. Thus, it was concluded that the electronic effect of R_1 and R_2 would influence the binding affinity of compounds with Nur77, R_1 and R_2 substituted with electron-donating group would enhance binding affinity of the compounds with Nur77. Besides, in the comparison of compound **13** with **13a** and **13c**, the substitution of R_3 and R_4 would weaken the binding affinity of compounds, which indicated that the steric hindrance of R_3 and R_4 would influence the binding affinity between compounds and Nur77, and that bulky group would impede the binding between compounds and Nur77. Overall, compound **13e**, in which R_1 was substituted with electron-giving group and R_3, R_4 showed no substitutions, displayed the best binding affinity to Nur77.

3.4. *In vitro binding evaluation of compound 13e with Nur77*

As mentioned above, compound **13e** exhibited the most potent binding affinity to Nur77, the calculated K_d is 0.54 ± 0.02 μM, as shown in Fig. 4**A**. The binding of compound **13e** to Nur77 was further evaluated by SPR assay (Fig. 4**B**, **Fig. S2**). SPR results indicated that the binding curve of compound **13e** showed a fast-on, fast-off kinetic pattern with a K_d value of 0.66 ± 0.21 μM. The result of SPR was consistent with fluorescence quenching assay (Fig. 4). In addition, we also measured the binding affinity of compound **13e** with Nurr1, which was the other member of NR4A family. The result showed that compound **13e** exhibited weak binding affinity with Nurr1 (**Fig. S4**). Collectively, all these data showed that compound **13e** directly binds to Nur77 *in vitro*. Therefore, compound **13e** was considered as a promising lead compound of this scaffold for the investigation of Nur77 related biological functions.

3.5. *Binding mode prediction of compound 13e*

To explore the molecular basis of binding affinity, molecular docking studies were performed. The predicted binding mode of compound **13e** in the binding site of Nur77 was compared with the X-ray co-crystal structure of the Nur77/THPN. As shown in Fig. 5, the binding position

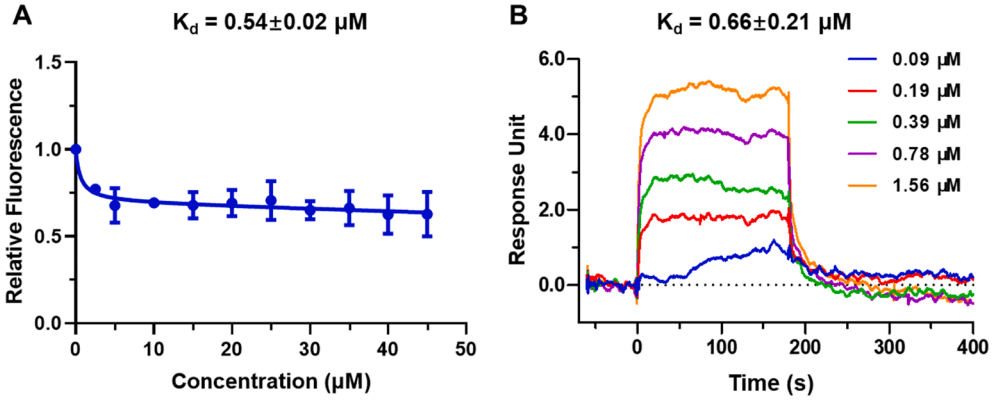

Fig. 4. Evaluation of the binding affinity of compound **13e** to Nur77 by *in vitro* assays. (A) Binding affinity measurement of compound **13e** to Nur77 by fluorescence quenching assay. Nur77-LBD was incubated with different concentrations of compound **13e** in assay buffer for 30 min at room temperature. The fluorescence intensity was measured at the excitation of 280 nm and the emission of 330 nm. Three independent experiments were carried out and the data was processed by GraphPad Prism 5.0. K_d was showed as mean ± SEM. (B) Binding affinity measurement of compound **13e** to Nur77 by SPR assay. Two independent experiments were carried out and the data was processed by Biocore T200 evaluation software. K_d was shown as mean ± SEM.

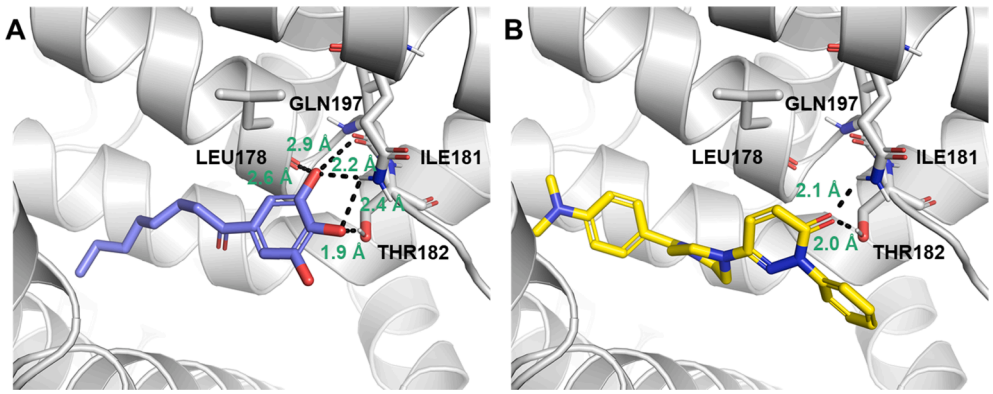

Fig. 5. Binding mode prediction and comparison of compound **13e** with THPN. (A) Crystal structure of Nur77-THPN complex (PDB: 4WHG). THPN was shown as a purple stick model. (B) Docking result showed the binding mode of compound **13e** in the binding pocket of Nur77. Compound **13e** was shown as a yellow stick model. Residues involved in the interaction were shown as sticks. Black dotted lines indicated the hydrogen-bonding interactions. (For interpretation of the references to colour in this figure legend, the reader is referred to the web version of this article.)

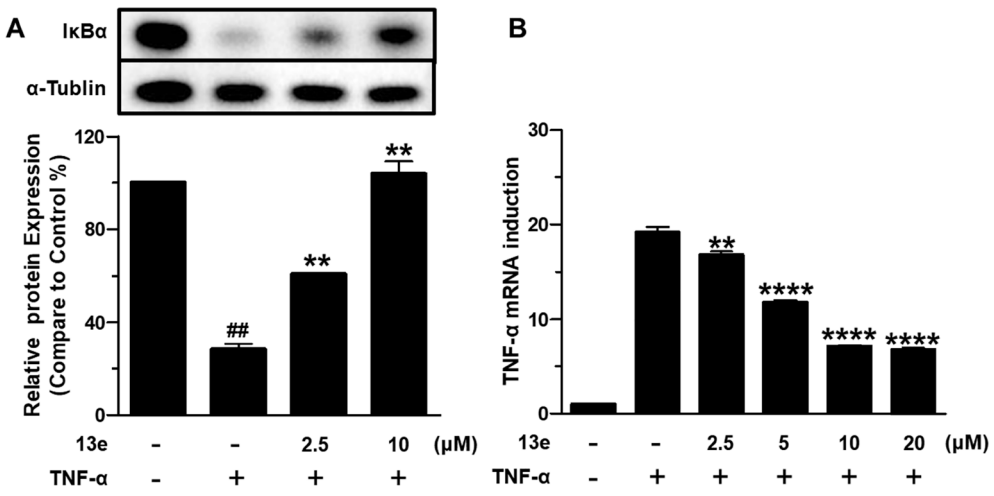

Fig. 6. Evaluation of the anti-inflammatory effect of compound **13e**. (A) IκBα degradation analysis of compound **13e**. HepG2 cells were treated with different concentrations of compound **13e** for 6 h and TNF-α (20 ng/mL) for 20 min, cell lysates were analyzed by western blotting and the results were processed by ImageJ. Statistical significance between the groups was determined using the *t*-test. The data are shown as mean ± SEM of two independent experiments. $^{**}P < 0.01$ vs the TNF-α group, $^{\#\#}P < 0.01$ vs the control group. (B) Inhibition of TNF-α in mRNA level by compound **13e**. HepG2 cells were treated with different concentrations of compound **13e** for 24 h and TNF-α (20 ng/mL) for 8 h, total RNA was isolated and analyzed by real-time quantitative PCR. The data are shown as the mean ± SEM of three independent experiments. $^{**}P < 0.01$ vs the control group, $^{****}P < 0.0001$ vs the control group.

of compound **13e** adopted an extended conformation and overlapped with the THPN-binding site (Fig. 5**B**), suggesting that the binding effect of compounds may result from occupation of the hydrophobic pocket of Nur77. The predicted position of 4-(dimethylamino)-benzene part of the compound **13e** was similar to the alkane chain at position 1 of THPN, generating Van Der Waals interaction with surrounding residues. In terms of Nur77-THPN, THPN formed three hydrogen bonds with LEU178, ILE181, and GLN197 via the hydroxyl oxygen atom at position 3 (2.6 Å, 2.2 Å, and 2.9 Å, respectively), and two hydrogen bonds with ILE181 and THR182 via the hydroxyl oxygen atom at position 4 (1.9 Å and 2.4 Å, respectively) (Fig. 5**A**). Among these aforementioned hydrogen bonding interactions, compound **13e** could form two hydrogen bonds with ILE181 and THR182 via carbonyl oxygen atom (2.1 Å and 2.0 Å, respectively) (Fig. 5**B**). The docking result indicated ILE181 and THR187 might be crucial to the binding of compound **13e** with Nur77. Moreover, it also suggests that interactions of small molecules with LEU178, ILE181, or GLN197 would provide beneficial guidance for the discovery of novel potent Nur77 targeting compounds. The binding mode analysis provided structural insight for future design and optimization of more efficient or specific Nur77 modulators.

3.6. Anti-inflammatory effects evaluation of compound 13e.

As reported, Nur77 could regulate the inflammation in HepG2 cells induced by TNF-α [18]. The anti-inflammatory effect of compound **13e** was detected in TNF-α induced HepG2 cell model. First, the cytotoxicity of compound **13e** on HepG2 cells was measured. Compound **13e** showed negligible cytotoxicity at the indicated concentrations (**Fig. S3**). The protection of IκBα degradation is a common marker to indicate the anti-inflammation activity of small molecules [19]. HepG2 cells were treated with compound **13e** and then the inflammation was induced by TNF-α. The protein expression level of IκBα was detected after compound **13e** treatment. The results showed that compound **13e** could significantly suppress the decrease of IκBα in a concentration-dependent manner (Fig. 6**A**). In addition, the expression of inflammatory cytokine TNF-α in mRNA level was also detected to verify the anti-inflammatory effects of compound **13e**. Consistent with the result of IκBα degradation, the increase of TNF-α mRNA level could also be remarkably inhibited by compound **13e** in a concentration-dependent manner (Fig. 6**B**). Therefore, the compound **13e** showed significant anti-inflammation activity on HepG2 cells.

To investigate the effect of compound **13e** on Nur77, we extracted the proteins of cytoplasm and nuclear respectively. Then, the protein amount of Nur77 was analyzed subsequently. The results showed Nur77 was increased in cytoplasm after treated with compound **13e** (**Fig. S5**). Therefore, it suggested that the action of compound **13e** on Nur77 resembled celastrol in HepG2 cells [18].

4. Conclusion

Nur77 plays a crucial role in the regulation of inflammatory processes. Modulation of Nur77 is a potential therapeutic approach for the treatment of inflammation-related diseases. In the present study, the evaluation of small molecule binding sites of Nur77 was carried out computationally. On this basis, the best scoring small molecule binding site was identified. Then, site-specific structure-based virtual screening was conducted on this best scoring site to discover novel small molecules of Nur77. Compound **13** was considered as the hit compound of Nur77 via protein thermal shift assay. According to the specific binding assay, compound **13** showed a K_d value of 4.03 ± 0.85 μM. Subsequently, 7 derivatives of compound **13** were obtained from the ChemDiv database by the similarity-based searching. Then compound **13e** were found to show the best binding affinity (K_d=0.54 ± 0.02 μM) of Nur77. Moreover, compound **13e** showed significant protection of IκBα degradation and inhibition of TNF-α in the mRNA level. Overall, in this study, we have evaluated all the small molecule binding sites in previously reported crystal structures, and discovered a series of anti-inflammatory Nur77 modulators with a novel scaffold via virtual screening. It provided a new insight into the biological function of specific small molecule binding sites of Nur77. These new scaffold compounds would serve as a starting point for further drug development targeting Nur77 for inflammation related diseases.

Declaration of Competing Interest

The authors declare that they have no known competing financial interests or personal relationships that could have appeared to influence the work reported in this paper.

Acknowledgement

We are grateful to National Centre for Protein Science Shanghai (Protein Expression and Purification system) for their instrument support and technical assistance. We gratefully acknowledge the financial supports from the China Postdoctoral Science Foundation (2020M681430 to H.X., and 2019M661673 to H.Z.), the National Natural Science Foundation of China (91853205, 81625022 to C.L., and 81903538 to H.Z.), National Science & Technology Major Project "Key

New Drug Creation and Manufacturing Program" of China (Number: 2018ZX09711002-001-003).

Appendix A. Supplementary material

Supplementary data to this article can be found online at https://doi.org/10.1016/j.bioorg.2021.104912.

References

[1] L. Pei, A. Castrillo, M. Chen, A. Hoffmann, P. Tontonoz, Induction of NR4A orphan nuclear receptor expression in macrophages in response to inflammatory stimuli, J. Biol. Chem. 280 (32) (2005) 29256–29262.

[2] A. Banno, S.P. Lakshmi, A.T. Reddy, S.C. Kim, R.C. Reddy, Key functions and therapeutic prospects of Nur77 in inflammation related lung diseases, Am. J. Pathol. 189 (3) (2019) 482–491.

[3] R. Rodríguez-Calvo, M. Tajes, M. Vázquez-Carrera, The NR4A subfamily of nuclear receptors: potential new therapeutic targets for the treatment of inflammatory diseases, Expert Opin. Ther. Targets 21 (3) (2017) 291–304.

[4] L. Wu, L. Chen, Characteristics of Nur77 and its ligands as potential anticancer compounds (Review), Mol. Med. Rep. (2018).

[5] Y. Zhan, X. Du, H. Chen, J. Liu, B. Zhao, D. Huang, G. Li, Q. Xu, M. Zhang, B. C. Weimer, D. Chen, Z. Cheng, L. Zhang, Q. Li, S. Li, Z. Zheng, S. Song, Y. Huang, Z. Ye, W. Su, S.C. Lin, Y. Shen, Q. Wu, Cytosporone B is an agonist for nuclear orphan receptor Nur77, Nat. Chem. Biol. 4 (9) (2008) 548–556.

[6] J. Liu, H. Zeng, L. Zhang, Y. Zhan, Y. Chen, Y. Wang, J. Wang, S. Xiang, W. Liu, W. Wang, H. Chen, Y. Shen, W. Su, P. Huang, H. Zhang, Q. Wu, A unique pharmacophore for activation of the nuclear orphan receptor Nur77 in vivo and in vitro, Cancer Res. 70 (9) (2010) 3628–3637.

[7] Y. Jiang, Y. Zeng, X. Huang, Y. Qin, W. Luo, S. Xiang, S.R. Sooranna, L. Pinhu, Nur77 attenuates endothelin-1 expression via downregulation of NF-κB and p38 MAPK in A549 cells and in an ARDS rat model, Am. J. Physiol. Lung Cell. Mol. Physiol. 311 (6) (2016) L1023–L1035.

[8] K. Palumbo-Zerr, P. Zerr, A. Distler, J. Fliehr, R. Mancuso, J. Huang, D. Mielenz, M. Tomcik, B.G. Fürnrohr, C. Scholtysek, C. Dees, C. Beyer, G. Krönke, D. Metzger, O. Distler, G. Schett, J.H.W. Distler, Orphan nuclear receptor NR4A1 regulates transforming growth factor-β signaling and fibrosis, Nat. Med. 21 (2) (2015) 150–158.

[9] S. Safe, S. Papineni, S. Chintharlapalli, Cancer chemotherapy with indole-3-carbinol, bis(3'-indolyl)methane and synthetic analogs, Cancer Lett. 269 (2) (2008) 326–338.

[10] E. Hedrick, S.O. Lee, S. Safe, The nuclear orphan receptor NR4A1 regulates beta1-integrin expression in pancreatic and colon cancer cells and can be targeted by NR4A1 antagonists, Mol. Carcinog. 56 (9) (2017) 2066–2075.

[11] S.O. Lee, X. Li, E. Hedrick, U.H. Jin, R.B. Tjalkens, D.S. Backos, L. Li, Y. Zhang, Q. Wu, S. Safe, Diindolylmethane analogs bind NR4A1 and are NR4A1 antagonists in colon cancer cells, Mol. Endocrinol. (Baltimore Md.) 28 (10) (2014) 1729–1739.

[12] A. Lacey, E. Hedrick, X. Li, K. Patel, R. Doddapaneni, M. Singh, S. Safe, Nuclear receptor 4A1 (NR4A1) as a drug target for treating rhabdomyosarcoma (RMS), Oncotarget 7 (21) (2016) 31257–31269.

[13] E. Hedrick, S.O. Lee, G. Kim, M. Abdelrahim, U.-H. Jin, S. Safe, A. Abudayyeh, Nuclear receptor 4A1 (NR4A1) as a drug target for renal cell adenocarcinoma, PLoS ONE 10 (6) (2015) e0128308.

[14] S.D. Cho, K. Yoon, S. Chintharlapalli, M. Abdelrahim, P. Lei, S. Hamilton, S. Khan, S.K. Ramaiah, S. Safe, Nur77 agonists induce proapoptotic genes and responses in colon cancer cells through nuclear receptor-dependent and nuclear receptor-independent pathways, Cancer Res. 67 (2) (2007) 674–683.

[15] S.O. Lee, X. Li, S. Khan, S. Safe, Targeting NR4A1 (TR3) in cancer cells and tumors, Expert Opin. Ther. Targets 15 (2) (2011) 195–206.

[16] S.D. Cho, S.O. Lee, S. Chintharlapalli, M. Abdelrahim, S. Khan, K. Yoon, A. M. Kamat, S. Safe, Activation of nerve growth factor-induced Bα by methylene-substituted diindolylmethanes in bladder cancer cells induces apoptosis and inhibits tumor growth, Mol. Pharmacol. 77 (3) (2010) 396–404.

[17] S.O. Lee, M. Abdelrahim, K. Yoon, S. Chintharlapalli, S. Papineni, K. Kim, H. Wang, S. Safe, Inactivation of the orphan nuclear receptor TR3/Nur77 inhibits pancreatic cancer cell and tumor growth, Cancer Res. 70 (17) (2010) 6824–6836.

[18] Hu M., Luo Q., Alitongbieke G., Chong S., Xu C., Xie L., Chen X., Zhang D., Zhou Y., Wang Z., Ye X., Cai L., Zhang F., Chen H., Jiang F., Fang H., Yang S., Liu J., Diaz-Meco M.T., Su Y., Zhou H., Moscat J., Lin X., Zhang X., Celastrol-Induced Nur77 Interaction with TRAF2 Alleviates Inflammation by Promoting Mitochondrial Ubiquitination and Autophagy, Mol Cell 66(1) (2017) 141–153 e6.

[19] Z. Chen, D. Zhang, S. Yan, C. Hu, Z. Huang, Z. Li, S. Peng, X. Li, Y. Zhu, H. Yu, B. Lian, Q. Kang, M. Li, Z. Zeng, X.K. Zhang, Y. Su, SAR study of celastrol analogs targeting Nur77-mediated inflammatory pathway, Eur. J. Med. Chem. 177 (2019) 171–187.

[20] Y. Chen, M. Jian, C. Lin, J. Kang, S. Chen, P. Lin, P. Hung, J. Chen, W. Chang, S. Lin, H. Harn, The induction of orphan nuclear receptor Nur77 expression by n-Butylenephthalide as pharmaceuticals on hepatocellular carcinoma cell therapy, Mol. Pharmacol. 74 (4) (2008) 1046–1058.

[21] P. Lin, Y. Chen, S. Chiu, Y. Yu, S. Chen, M. Chien, K. Chen, W. Chang, S. Lin, T. Chiou, H. Harn, Orphan nuclear receptor, Nurr-77 was a possible target gene of butylidenephthalide chemotherapy on glioblastoma multiform brain tumor, J. Neurochem. 106 (3) (2008) 1017–1026.

[22] P. Liu, J. Sheu, P. Lin, C. Lin, Y. Liu, L. Ho, L. Chang, W. Wu, S. Chen, J. Chen, Y. Harn, S. Lin, C. Tsai, T. Chiou, H. Harn, Expression of Nur77 induced by an n-butylidenephthalide derivative promotes apoptosis and inhibits cell growth in oral squamous cell carcinoma, Invest. New Drugs 30 (1) (2012) 79–89.

[23] L. Chang, P. Lin, L. Ho, P. Liu, W. Wu, I. Chiang, H. Chang, S. Lin, Y. Harn, H. Harn, T. Chiou, Overexpression of the orphan receptor Nur77 and its translocation induced by PCH4 may inhibit malignant glioma cell growth and induce cell apoptosis, J. Surg. Oncol. 103 (5) (2011) 442–450.

[24] Y. Zhan, Y. Chen, Q. Zhang, J. Zhuang, M. Tian, H. Chen, L. Zhang, H. Zhang, J. He, W. Wang, R. Wu, Y. Wang, C. Shi, K. Yang, A. Li, Y. Xin, T. Li, J Yang, Z. Zheng, C. Yu, S. Lin, C. Chang, P. Huang, T. Lin, Q. Wu, The orphan nuclear receptor Nur77 regulates LKB1 localization and activates AMPK, Nat. Chem. Biol. 8 (11) (2012) 897–904.

[25] M.A. Pearen, J.G. Ryall, M.A. Maxwell, N. Ohkura, G.S. Lynch, G.E. Muscat, The orphan nuclear receptor, NOR-1, is a target of beta-adrenergic signaling in skeletal muscle, Endocrinology 147 (11) (2006) 5217–5227.

[26] W. Wang, Y. Wang, H. Chen, Y. Xing, F. Li, Q. Zhang, B. Zhou, H. Zhang, J. Zhang, X. Bian, L. Li, Y. Liu, B. Zhao, Y. Chen, R. Wu, A. Li, L. Yao, P. Chen, Y. Zhang, X. Tian, F. Beermann, M. Wu, J. Han, P. Huang, T. Lin, Q. Wu, Orphan nuclear receptor TR3 acts in autophagic cell death via mitochondrial signaling pathway, Nat. Chem. Biol. 10 (2) (2014) 133–140.

[27] L. Li, Y. Liu, H. Chen, F. Li, J. Wu, H. Zhang, J. He, Y. Xing, Y. Chen, W. Wang, X. Tian, A. Li, Q. Zhang, P. Huang, J. Han, T. Lin, Q. Wu, Impeding the interaction between Nur77 and p38 reduces LPS-induced inflammation, Nat. Chem. Biol. 11 (5) (2015) 339–346.

[28] W. Wang, Y. Wang, P. Hou, F. Li, B. Zhou, H. Chen, X. Bian, Q. Cai, Y. Xing, J. He, H. Zhang, P. Huang, T. Lin, Q. Wu, Induction of autophagic death in cancer cells by agonizing TR3 and attenuating Akt2 activity, Chem. Biol. 22 (8) (2015) 1040–1051.

[29] P. Yang, P. Hou, F. Liu, W. Hong, H. Chen, X. Sun, P. Li, Y. Zhang, C. Ju, L. Luo, S. Wu, J. Zhou, Z. Wang, J. He, L. Li, T. Zhao, X. Deng, T. Lin, Q. Wu, Blocking PPARγ interaction facilitates Nur77 interdiction of fatty acid uptake and suppresses breast cancer progression, Proc. Natl. Acad. Sci. U.S.A. 117 (44) (2020) 27412–27422.

[30] J.C. Shelley, A. Cholleti, L.L. Frye, J.R. Greenwood, M.R. Timlin, M. Uchimaya, Epik: a software program for pKa prediction and protonation state generation for drug-like molecules, J. Comput. Aided Mol. Des. 21 (12) (2007) 681–691.

[31] B. Zhao, H. Chen, N. Lei, G. Li, W. Zhao, Y. Zhan, B. Liu, S. Lin, Q. Wu, p53 mediates the negative regulation of MDM2 by orphan receptor TR3, EMBO J. 25 (24) (2006) 5703–5715.

[32] T.A. Halgren, Identifying and characterizing binding sites and assessing druggability, J. Chem. Inf. Model. 49 (2) (2009) 377–389.

[33] M. Nayal, B. Honig, On the nature of cavities on protein surfaces: application to the identification of drug-binding sites, Proteins 63 (4) (2006) 892–906.

[34] T. Halgren, New method for fast and accurate binding-site identification and analysis, Chem. Biol. Drug Des. 69 (2) (2007) 146–148.

[35] U. Cogan, M. Kopelman, S. Mokady, M. Shinitzky, Binding affinities of retinol and related compounds to retinol binding proteins, Eur. J. Biochem. 65 (1) (1976) 71–78.

[36] C. Bodenreider, D. Beer, T.H. Keller, S. Sonntag, D. Wen, L. Yap, Y.H. Yau, S. G. Shochat, D. Huang, T. Zhou, A. Caflisch, X.C. Su, K. Ozawa, G. Otting, S. G. Vasudevan, J. Lescar, S.P. Lim, A fluorescence quenching assay to discriminate between specific and nonspecific inhibitors of dengue virus protease, Anal. Biochem. 395 (2) (2009) 195–204.